J Mater Sci (2022) 57:204–216

Ceramics

Engineering *A*-site cation deficiency into $LaCoO_3$ thin sheets for improved microwave absorption performance

Yingrui Feng[1], Kang Hu[1], Min Zhang[1], Wei Ding[2,3], Xiangkai Kong[1,*], Zhigao Sheng[2,*], and Qiangchun Liu[1,*]

[1] Anhui Province Key Laboratory of Pollutant Sensitive Materials and Environmental Remediation, School of Physics and Electronic Information, Huaibei Normal University, Huaibei 235000, People's Republic of China
[2] High Magnetic Field Laboratory, Chinese Academy of Sciences, Hefei 230031, People's Republic of China
[3] Institutes of Physical Science and Information Technology, Anhui University, Hefei 230601, People's Republic of China

Received: 9 August 2021
Accepted: 20 October 2021
Published online: 3 January 2022

ABSTRACT

Rationally designing microwave absorption materials with highly efficient and tunable bandwidth is in great demand but remains a huge challenge. In this study, perovskite oxide $LaCoO_3$ thin sheets have been obtained by the hydrothermal synthesis and subsequent annealing process. Then, cation deficiency is introduced to the *A*-site of $LaCoO_3$ via a selectively etching strategy by $FeCl_3$ solution. The phase characteristics, morphologies, structures, and microwave absorption performance of $LaCoO_3$ thin sheets with *A*-site cation deficiency have been systematically investigated. The results indicate that a suitable introduction of the *A*-site cation deficiency is beneficial to induce more dipole polarization, leading to the enhancement of the microwave absorption performance. When the amount of $FeCl_3$ is 0.3 g, the $LaCoO_3$ thin sheets exhibited superior reflection loss characteristics in the range of test frequency. Exhilaratingly, a minimum reflection loss (RL) value of − 56.9 dB at 15.1 GHz can be achieved with a thin thickness of 2.0 mm. Meanwhile, a broad effective absorption bandwidth reaches 5.9 GHz, covering the range of 12.1–18.0 GHz. It is believed that introducing the *A*-site cation deficiency of $LaCoO_3$ can be used as an effective means for tuning microwave absorption.

Handling Editor: David Cann.

Address correspondence to E-mail: kxk@chnu.edu.cn; zhigaosheng@hmfl.ac.cn; zhigaosheng@gmail.com; qchliu@chnu.edu.cn
E-mail Addresses: fengyingrui2021@126.com; khu_hsd@163.com; zmin@mail.ustc.edu.cn; weiding@mail.ustc.edu.cn

https://doi.org/10.1007/s10853-021-06650-2

Introduction

Recently, electromagnetic (EM) interference has become the most severe concern in current society because of the explosive development of information technology and more unwanted EM irradiations generate problems of environmental pollution [1–4]. As a crucial functional material, microwave absorption material can efficiently dissipate EM waves and successfully transform EM energy to thermal or other energy, which has been regarded as an effective solution to solve the EM irradiation problem [5, 6]. Therefore, construction of the EM wave absorbing materials with high-efficiency, wide absorption frequency range, small thickness, and lightweight have been actively pursued in practical applications [7–9]. Until now, numerous microwave absorption materials include dielectric materials, magnetic materials, conductive polymers, and carbonaceous materials that have been investigated taking into account their outstanding dielectric and magnetic characteristics [10–13]. Customarily, multi-component materials were selected as microwave absorbing materials due to the single component materials were usually limited by the impedance mismatch and the narrow effective absorption bandwidth. Under these circumstances, much effort has been devoted to searching for new microwave absorbers. For example, Liu et al. constructed ellipsoid-like $MgCo_2O_4$/Co_3O_4 composites through a facile hydrothermal method and heat treatment, and they found that the calcination temperature is crucial for crystalline structure and microwave absorption performance [14]. Cui et al. constructed 1D customized heterogeneous structure of Fe_3N@C that gained a strong electromagnetic wave response [15]. Wang et al. activated excellent microwave absorption performance via building π-π stacking heterostructure with small organic molecules [16].

As a kind of important ABO_3-perovskite oxides, $LaCoO_3$ has been attracted widespread attention due to its high electron mobility and diverse chemical properties [17–19]. For example, Sun et al. synthesized porous $La_{0.9}Co_{0.8}Ni_{0.2}O_{3-x}$ nanocubes by a facile hydrothermal method, which was explored to be a promising bifunctional OER and ORR catalyst for LiO_2 batteries [20]. Liu and co-workers demonstrated that the treatment of pristine $LaCoO_3$ with Ar plasma to introduce oxygen vacancies for $LaCoO_3$, which showed a higher selectivity toward N_2 electroreduction [21]. Thus, inducing deficiency or *A*-site/*B*-site cation substitution in perovskites can be regarded as an effective means to regulate the crystal structure, which is beneficial to improve their unique physical and chemical properties. More importantly, *A*-site deficiency can introduce oxygen vacancies to tune the electronic structure and increase electrical conductivities in perovskite oxides [22, 23].

Herein, an efficient microwave absorber of $LaCoO_3$ thin sheets with *A*-site deficiency was synthesized by $FeCl_3$ post-treatment. In detail, $LaCoO_3$ thin sheets have been obtained by a hydrothermal reaction and subsequent annealing process. Then, *A*-site deficiency was further introduced to $LaCoO_3$ by $FeCl_3$ selectively dissolve La cations, resulting in boosted microwave absorption properties. To the best of our knowledge, there is no report regarding introducing *A*-site deficiency into $LaCoO_3$ perovskite to enhance its microwave absorption properties. The $LaCoO_3$ thin sheets with *A*-site deficiency exhibit a substantially enhanced microwave absorption performance with the minimum reflection loss (RL_{min}) of − 56.9 dB at 15.1 GHz and a 5.9 GHz bandwidth with RL less than − 10 dB is achieved. In brief, the proposed *A*-site deficiency strategy indicates that dielectric polarization is dominant in determining the permittivity behaviors in perovskite. This study will offer new insights for designing highly efficient perovskite applied in the microwave absorption field.

Experimental sections

Materials

The cobalt nitrate hexahydrate ($Co(NO_3)_2{\cdot}6H_2O$), lanthanum nitrate hexahydrate ($La(NO_3)_3{\cdot}6H_2O$), urea ($CO(NH_2)_2$), potassium hydroxide (KOH), and ferric chloride hexahydrate ($FeCl_3{\cdot}6H_2O$) were all purchased from Shanghai Sinopharm Chemical Reagents Co., Ltd. All chemical reagents were commercially available and used without any further purification.

Fabrication of two-dimensional $LaCoO_3$ thin sheets

In a typical process, 2 mmol $La(NO_3)_3{\cdot}6H_2O$, 2 mmol $Co(NO_3)_2{\cdot}6H_2O$ and 0.2 g $CO(NH_2)_2$ were dissolved

in 40 mL deionized water under vigorous stirring until the solution becomes transparent, then 15 mmol KOH was added to the transparent solution and pink precipitation is formed immediately. After that, the mixture was stirred for 2 h and the precipitations were translated to gray-brown. Then the above solution was transferred into the 50 mL Teflon-lined autoclave for hydrothermal treatment at 200 °C for 12 h. Subsequently, the reaction system was naturally cooled to room temperature, and the precursors were centrifuged and washed several times with water and ethanol and then dried at 60 °C for 12 h in a vacuum. Finally, the as-prepared precursors were calcined at 800 °C for 2 h with a heating rate of 5 °C·min^{-1} in an air atmosphere.

Fabrication of *A*-site cation deficiency for $LaCoO_3$ thin sheets

Typically, the as-prepared $LaCoO_3$ (0.1 g) were dispersed in 20 mL deionized water before injecting the different amounts of $FeCl_3$, the etching process was conducted for 2 h under vigorous stirring. The suspension solution was collected by centrifugation, then washed with deionized water and ethanol, and dried at 80 °C for 12 h. The final products were denoted as S1, S2, S3, and S4, corresponding to 0, 0.1 g, 0.3 g, and 0.5 g $FeCl_3$, respectively.

Characterization

The crystal structure and crystallinity of the samples were characterized by X-ray powder Diffraction (XRD) with Cu Kα radiation source (40.0 kV, 40.0 mA λ = 1.5406 Å) in the range from 2θ = 10° to 70°. The morphology and structure of the samples were investigated by field emission scanning electron microscopy (FESEM, SU8220) and the transmission electron microscopy (TEM, JEOL JEM-2100). The element chemical state was recorded on X-ray photoelectron spectroscopy (XPS) AXIS Supra with a monochromatic X-ray source.

Electromagnetic parameters measurement

Electromagnetic parameters were measured using a vector network analyzer (VNA, AV629D) in the frequency range of 2–18 GHz. Before the Electromagnetic parameter test, the samples were uniformly dispersed in paraffin wax with a mass fraction of 60% and then compacted into a columnar ring of 7.00 mm out diameter and 3.04 mm inner diameter. Generally, the electromagnetic wave absorbing performance of the samples can be evaluated by the reflection loss (RL), which can be defined by the following equations on the basis of transmission line theory [24, 25]:

$$\mathrm{RL}\ (\mathrm{dB}) = 20\log|(Z_{\mathrm{in}} - Z_0)/(Z_{\mathrm{in}} + Z_0)| \quad (1)$$

$$Z_{\mathrm{in}}/Z_0 = \sqrt{\mu_r/\varepsilon_r}\tanh\left[j(2\pi fd/c)\sqrt{\mu_r\varepsilon_r}\right] \quad (2)$$

where RL is the reflection loss coefficient, Z_{in} is the input impedance of the absorbers, Z_0 is the impedance of free space, c is the velocity of light, f is the frequency of microwave in free space and d is the coating thickness. Usually, the absorbers are required to have RL values less than − 10 dB, which means 90% of the incident electromagnetic wave is absorbed and the frequency ranges are defined as effective absorption band (EAB) [26].

Results and discussion

In order to understand the experimental process more clearly, the fabrication procedure for $LaCoO_3$ thin sheet with *A* cation deficiency is schematically depicted in Fig. 1. $LaCoO_3$ precursors are firstly obtained through a facile hydrothermal method, and the as-prepared precursors are further converted into $LaCoO_3$ thin sheets under the air atmosphere at high temperatures. Then the samples were immersed in a $FeCl_3$ solution with stirring vigorously. $FeCl_3$ was selected as the modulation solution for the moderate acidity of Fe^{3+} to selectively dissolve La elements and preferentially deposit Fe ions on the corroded $LaCoO_3$ surface[27]. Due to the continual leaching of the La^{3+}, the crystalline structure of perovskite collapsed progressively and became amorphous.

XRD is introduced to investigate the crystalline structures and phase purity of the samples obtained with different masses of $FeCl_3$ in a 2θ range between 10° and 70°, as shown in Fig. 2a. The XRD curve of the as-prepared S1 presents sharp and strong diffraction peaks show the $LaCoO_3$ are high-purity nanocrystal, which could be well indexed to the (012), (110), (104), (113), (202), (211), (006), (024), (122), (116), (300), (214), (018), (220) and (208) planes, respectively. All the diffraction peaks are consistent with the standard card (JCPDS No 48-0123) of perovskite-structured $LaCoO_3$ [28]. After etching by $FeCl_3$, there

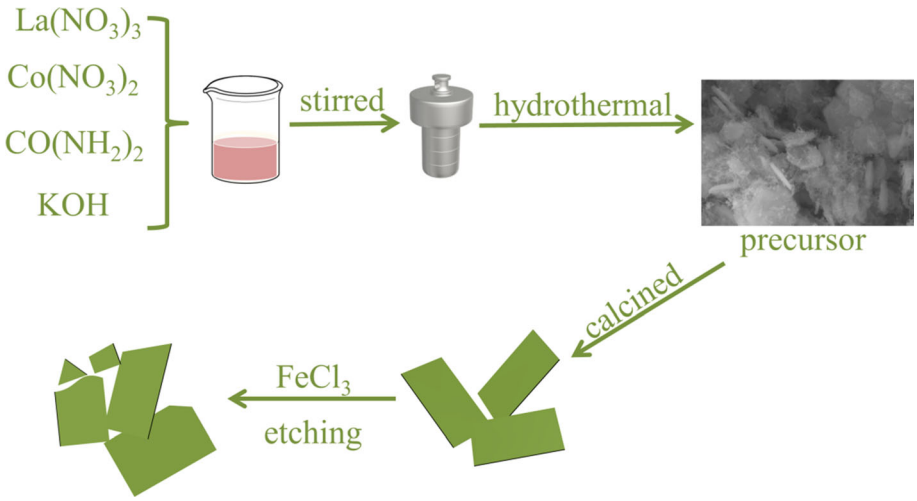

Figure 1 Schematic illustration of the fabrication process for LaCoO3 thin sheets with A-site cation deficiency.

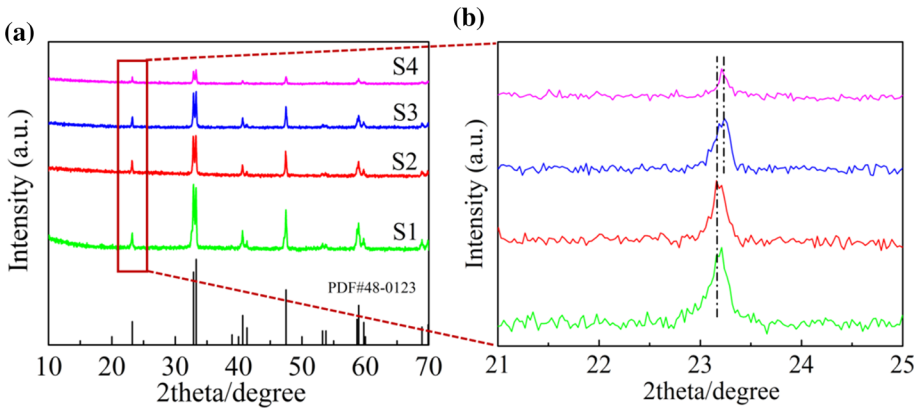

Figure 2 XRD patterns of **a** the obtained $LaCoO_3$ samples at different etching conditions and **b** partially enlarged view of picture (**a**).

was no significant change in the diffraction peaks (iron oxide) compared with that of $LaCoO_3$. These results indicate that the crystalline structure of $LaCoO_3$ remains in its original state after the $FeCl_3$ etch. However, it is clearly seen that the XRD diffraction peak intensity of the samples decreases remarkably with the increase of $FeCl_3$ and some weak diffraction peaks have been covered under the strong etching condition. Furthermore, the lack of larger ionic La sited at the A position, the crystal lattice is partly shrunk. When introducing the La deficiency, it can be observed that a slight shift in the diffraction peaks toward higher angles compared to the pristine $LaCoO_3$ as shown in Fig. 2b and [29].

The morphologies and structure of as-synthesized samples are characterized by field emission scanning electron microscopy (FESEM) and transmission electron microscopy (TEM), as displayed in Fig. 3a–d. The FESEM image of S1 shows uniform sheet morphology with a thickness of 227 nm. It is clearly seen that the thin sheets show a collapse tendency along with the increase of $FeCl_3$. After 0.1 g and 0.3 g $FeCl_3$ etching treatment, a small amount of $LaCoO_3$ thin sheets has been destroyed into particles. When the mass of $FeCl_3$ increases to 0.5 g, most of the flakiness has been destroyed. The morphology of the $LaCoO_3$ precursor obtained by the hydrothermal process is formed in Fig. S1. Meanwhile, the elemental mapping was used to confirm the corresponding elemental distribution for S1 and S3. The La, Co, and O elements almost spread among the whole test area, as shown in Fig. 3e–f. And more notably, the Fe element also demonstrates a homogeneous distribution in S3. In order to further quantitative analysis of these elements, the energy-dispersive X-ray spectroscopy (EDS) is used to verify the distribution of these elements. The EDS data are shown in Fig. S2. It can be seen the presence of a small amount of Fe element after etching condition. But the content of iron ions did not increase significantly with the adding of $FeCl_3$, indicating that the iron ions mainly play an etching role. As shown in Fig. 3g–i, more detailed

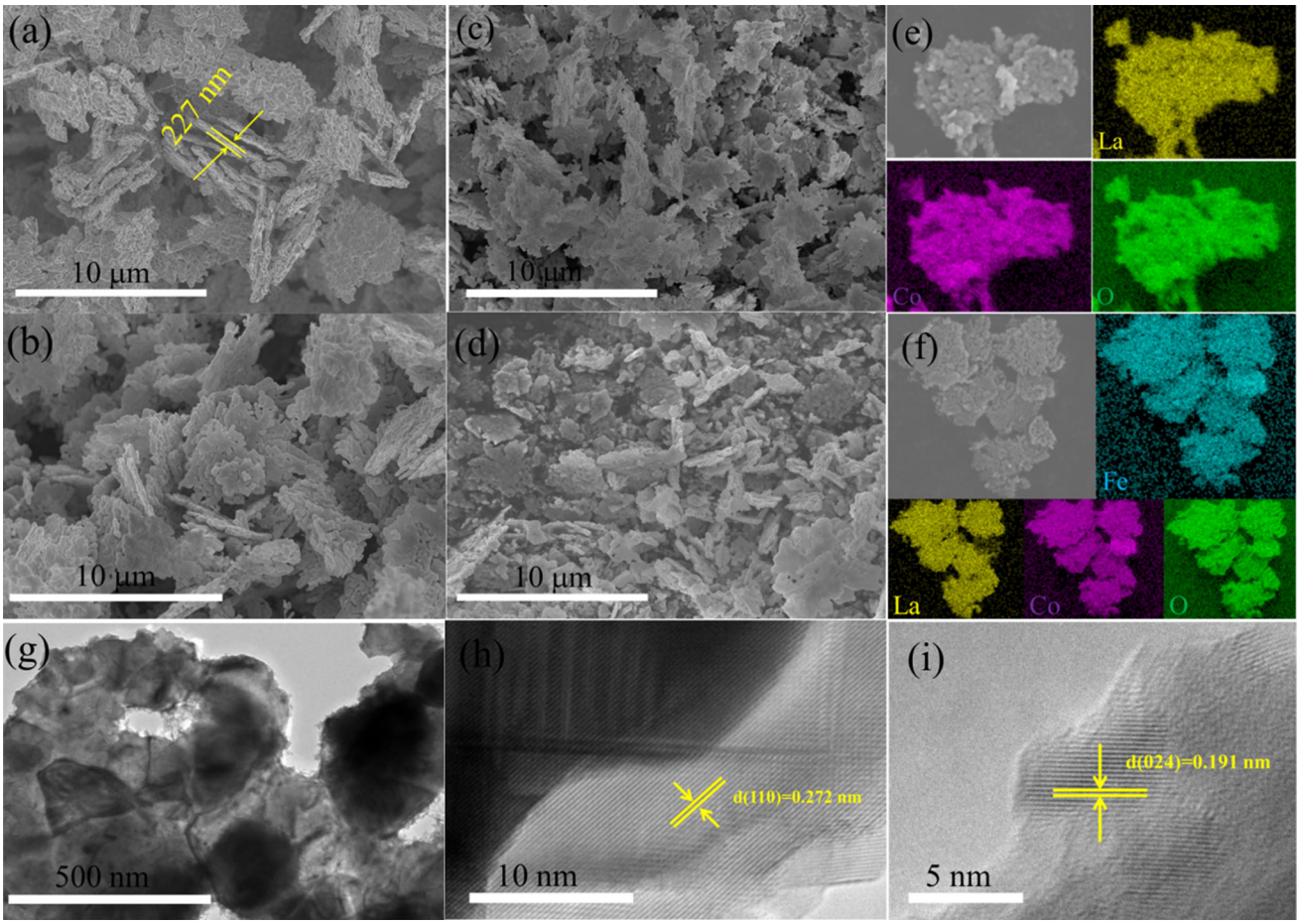

Figure 3 FSEM images of **a** S1, **b** S2, **c** S3 and **d** S4; **e**–**f** the element mapping for S1 and S3. TEM and HRTEM images of S3 (**g**–**i**).

information on the structure of S3 is investigated by TEM. Figure 3h–i shows the lattice fringes with interplanar spaces of 0.272 and 0.191 nm, which correspond to the (110) and (024) planes of $LaCoO_3$ nanocrystals with perovskite structure, respectively.

The surface chemical element composition of the pristine $LaCoO_3$ (S1) and after etching by 0.3 g $FeCl_3$ (S3) are explored by X-ray photoelectron spectroscopy (XPS) in Fig. 4. As displayed in Fig. 4a, the binding energy (BE) peaks of La 3d are centered at 851.6 and 834.8 eV can be assigned to the La 3*d*5/2 and 3*d*3/2, respectively. The satellites peaks at 855.7 and 838.9 eV can be attributed to the shake-up states of La 3*d* due to the electron transition from the O 2*p* valence bands to La 4*f* orbits [30]. Figure 4b shows the Co 2*p* fitting curves, which contains 2*p*3/2 and 2*p*1/2 peaks are located at 795 and 779.4 eV [31]. The BE peaks of Fe 2*p* are depicted in Fig. S3. It is seen that the O 1 s XPS spectra of two samples (S1 and S3) are wide and asymmetric, which can be break up into three and four kinds of oxygen species, respectively. As displayed in Fig. 4c, the O1 peak at 533.5 eV is attributed to the physical or chemical absorber molecular water. The O2 peak at BE of 530.8 eV indicated the presence of the surface chemisorbed oxygen. The relatively strong peak at BE of 528.3 eV represented the lattice oxygen species, which is ascribed from the contribution of La–O and Co–O in the crystal lattice. More importantly, when the cation deficiency is introduced to the *A*-site of $LaCoO_3$, the O3 peak is weakened, and it generates a new peak O4 at binding energy (BE) of 529.2 eV, which indicate the oxygen vacancies have been produced in the perovskite $LaCoO_3$ thin sheets surface [32], as shown in Fig. 4d. This phenomenon proves the etching effect of the $FeCl_3$ solution on the $LaCoO_3$ surface to introduce oxygen vacancies, which play an important role in the enhancement of dipoles polarization.

The relative complex permittivity ($\varepsilon_r = \varepsilon' - j\varepsilon''$) and permeability ($\mu_r = \mu' - j\mu''$) of the microwave

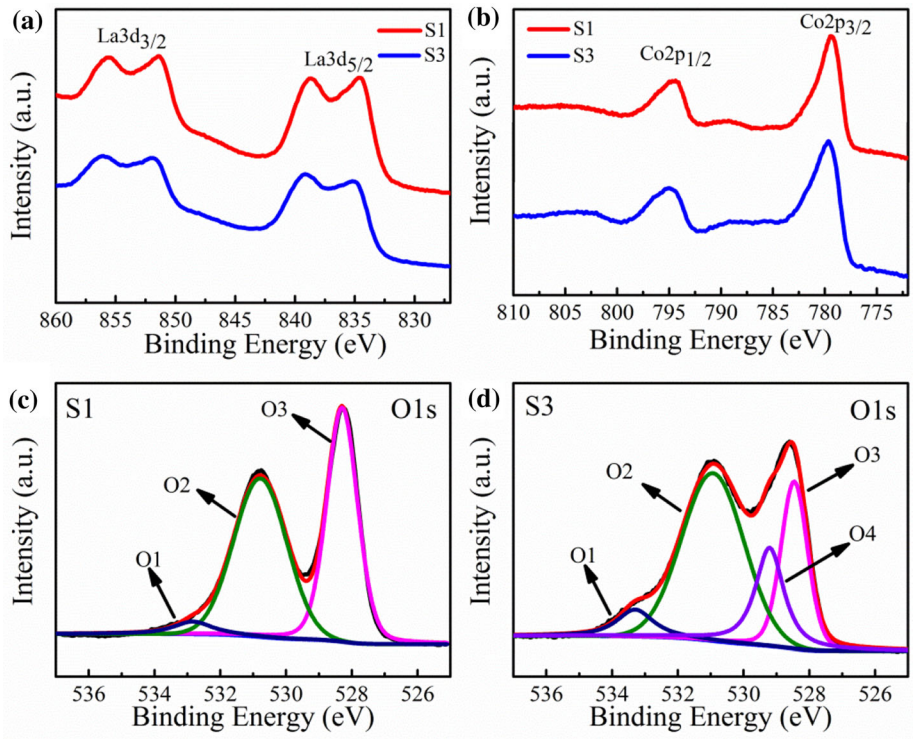

Figure 4 The XPS spectra of La3d (**a**), Co2p (**b**), and O1s regions of S1 and S3(**c**) (**d**), respectively.

absorption materials usually play two vitally important roles in determining the microwave absorption. The real part ε' and μ' represent the storage capacity of electrical and magnetic energy, while the imaginary part ε'' and μ'' are related to dissipation (or loss) of electrical and magnetic energy [33, 34], respectively. In this work, the electromagnetic properties of the as-prepared samples are investigated in the frequency range of 2–18 GHz, as shown in Fig. 5. The μ' and μ'' values of all of the $LaCoO_3$ samples were nearly close to 1 and 0 (as shown in Fig. S4). It demonstrates that the microwave absorption performance of the $LaCoO_3$ thin sheet with *A*-site cation deficiency is mainly attributed to the dielectric loss. As displayed in Fig. 5a, the four samples exhibit distinct ε' and the ε' values of all samples decrease as the frequency increases, which means a typical frequency dispersion behavior. The values of ε' are in the range of 7.1–4.1, 9.8–5.3, 11.9–6.2, and 10.8–5.4 for S1, S2, S3, and S4, respectively. And the values of ε'' in Fig. 5b are in the range of 2.5–1.5, 3.8–2.1, 4.1–3.1, and 3.7–2.4, which correspond to S1, S2, S3, and S4, respectively. Obviously, the ε' and ε'' values of S1 remained a low level with the variation of frequency, indicating the poorest storage and dissipation capability. As the increase of Fe^{3+}, the real part of the permittivity has a tendency to increase first and then decrease, which indicates that the etching effect of Fe^{3+} has a favorable adjustment for the dielectric storage capability of the absorber. As the increase of

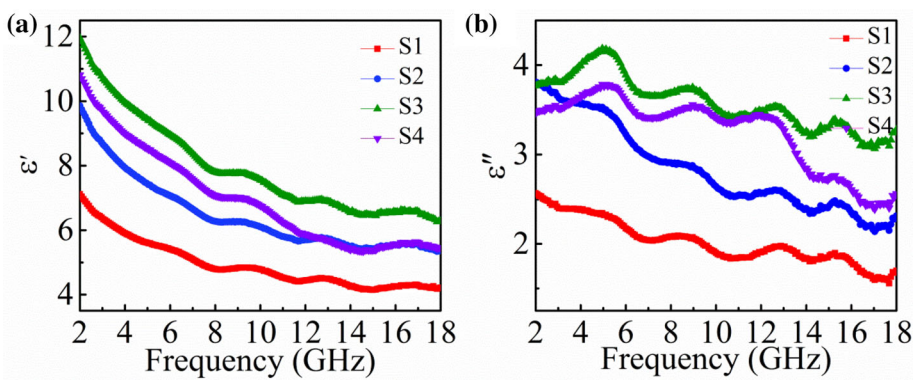

Figure 5 Frequency dependence of the real part (ε′) (**a**), imaginary part (ε″) (**b**) of permittivity.

Fe^{3+}, the change in the imaginary part of the permittivity over the entire test frequency range is consistent with the real part of the dielectric. But the imaginary part of the samples has multiple strong polarization resonance which can attribute to the interface polarization and dipoles polarization caused by the defects of oxygen in the test frequency range[35]. For further evaluating the dielectric loss strength of all samples, the dielectric tangent loss ($\tan\delta_\varepsilon = \varepsilon''/\varepsilon'$) can be evaluated for the electromagnetic dissipation. As shown in Fig. S5, the samples of S4 possess a relatively higher tangent value in the range of 6.88–18 GHz, indicating the strongest dielectric loss capability. But, as shown in Fig. 7e and Fig. 3, the impedance matching and the sheet structure of S3 is much better than S4, which means that S3 has the most excellent EMW absorption performance.

With the aim to evaluate the microwave absorption performance of the as-prepared samples, the corresponding three-dimensional and two-dimensional contour maps of the RL are calculated by the transmission line theory, as described in Fig. 6. Clearly, the perovskite oxide $LaCoO_3$ thin sheets exhibit the different performance of microwave absorption at different etching conditions. As shown in Fig. 6a, the original $LaCoO_3$ (S1) shows a poor microwave absorption capability with only a minimum RL of − 14.9 dB at the thickness of 2.5 mm. Meanwhile, adjusting the lattice imperfection by Fe^{3+} etching, the microwave absorption performance of the samples is significantly enhanced. For the S2, the minimum RL values reached − 42.2 dB with a thickness of 5.0 mm, showing high-performance microwave absorption but the sample is thick, which is not suitable for practical application (Fig. 6b). Moreover, the S3 has excellent microwave absorption properties that the optimum RL is − 56.9 dB at 15.1 GHz, and a wide EAB of 5.9 GHz can be achieved in the range of 12.1–18.0 GHz, almost covering K_u band at only 2.0 mm, as exhibited in Fig. 6c. However, the further increase in sample etching conditions leads to a decrease in microwave absorption performance. The S4 possesses a minimum RL is − 35.7 dB at 4.88 GHz with a thickness of 5.0 mm, which is similar to that of S2, but a narrow EAB of 2.4 GHz (Fig. 6d). In general, S3 has the characteristics of strong absorption, thin thickness, and broad bandwidth, which is consistent with the 2D plots of the RL values (Fig. 6e–h). Therefore, $LaCoO_3$ thin sheets with *A*-site cation deficiency can be controlled optimized, with the moderate concentration of Fe^{3+} to selectively dissolve La elements in the perovskite structure, and thus lead to the boosted of the microwave absorption performance.

Furthermore, in order to directly compare the microwave absorption performance of the $LaCoO_3$ thin sheets with *A*-site cation deficiency, the RL_{min} value and the EAB are summarized in Fig. 7. The microwave absorption performance of the as-obtained S3 outperforms other samples according to the combination of thickness, broad EAB, and RL, which can be used as an effective means for tuning microwave absorption.

Generally, the permittivity of materials results from various kinds of polarization, including interfacial polarization, dipolar polarization, electron polarization, and ionic polarization[36]. However, the polarization of electrons and ions can be neglected because they occur in the ultraviolet and infrared band [37]. Therefore, interface and dipole polarization should be the main types of polarization in this case. To further understanding the polarization effect during the microwave absorption process, the relationship of ε' and ε'' can be elucidated by Debye theory in the following equation [38, 39]:

$$\left(\varepsilon' - \frac{\varepsilon_s + \varepsilon_\infty}{2}\right) + (\varepsilon'')^2 = \left(\frac{\varepsilon_s - \varepsilon_\infty}{2}\right)^2 \quad (3)$$

where ε_s and ε_∞ are static permittivity and permittivity at the infinite frequency, respectively. Hence, the semicircle in the plots of ε' to ε'' stands for a Debye relaxation process which is related to polarization in the studied frequency range[40]. As shown in Fig. 8a–d, all the samples have multiple semicircles in the plots of ε' to ε'', manifesting the presence of multiple Debye relaxing processes, which is caused by the interfacial polarization and dipolar polarization in these samples. This phenomenon further proves that the multi-dielectric relaxation is beneficial to enhancing microwaves absorption properties[41]. To deeply understand the dielectric behavior of the $LaCoO_3$ thin sheets with *A*-site cation deficiency, the variation of the complex permittivity of these samples can be explained in detail. It is worth pointing out that a long tail is associated with the conduction loss in the plots of ε' to ε'' [42]. Furthermore, the tail becomes short as the mass of $FeCl_3$ increased. These phenomena indicate that the conduction loss may gradually weaken and the polarization loss is enhanced because the existence of iron ions remained

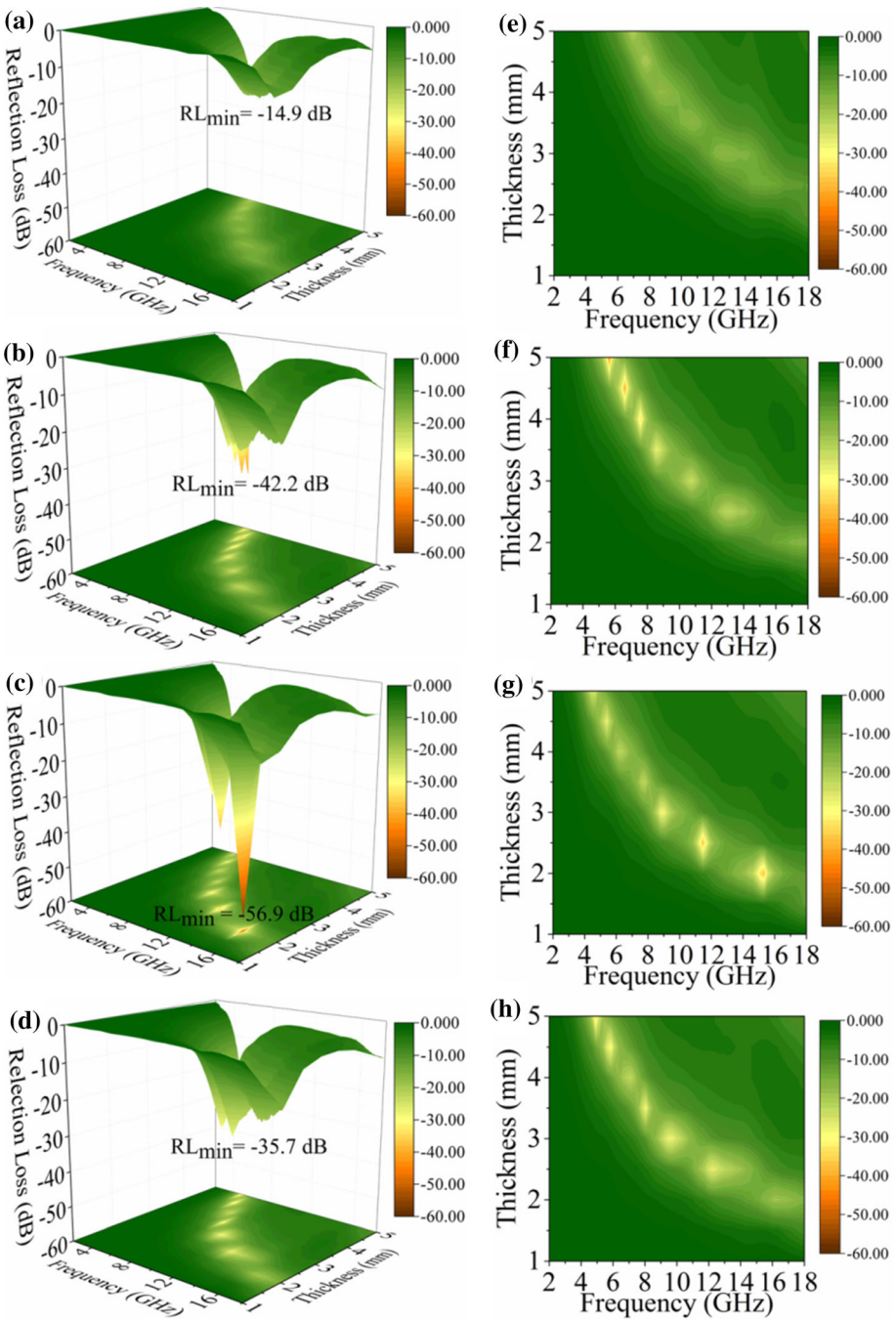

Figure 6 Three-dimensional and two-dimensional RL plots map of S1 (**a**, **e**), S2 (**b**, **f**), S3(**c**, **g**), and S4 (**d**, **h**).

leads to stronger interface polarization. Also, the etching of iron ions makes the sample have more defects which play the role of the center of dipoles polarization, resulting in more dipole polarization. Therefore, the above results revealed the existence of three primary factors including dipole polarization, interfacial polarization, and conduction loss, which were in favor of the dielectric loss. In the previous study, dielectric polarization plays a dominant role in determining the permittivity behaviors in semiconductors due to the limited conductive capability of semiconductor materials [43]. The polarization and conduction loss have opposite on the permittivity behaviors of semiconductors. When this perovskite material is etched by $FeCl_3$, dielectric loss is mainly attributed to the polarization effect.

Generally, two indispensable factors should be taken into consideration while aiming to achieve

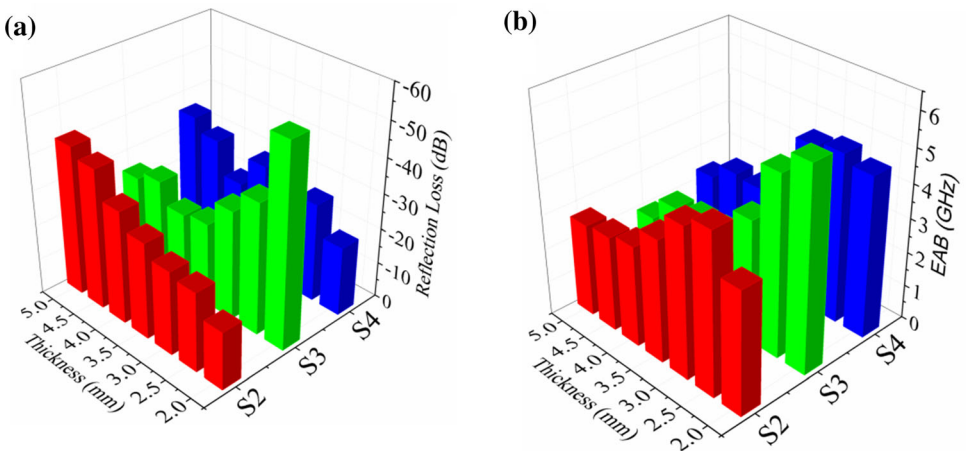

Figure 7 RLmin values (**a**) and EAB (**b**) of as-prepared $LaCoO_3$ at different thicknesses.

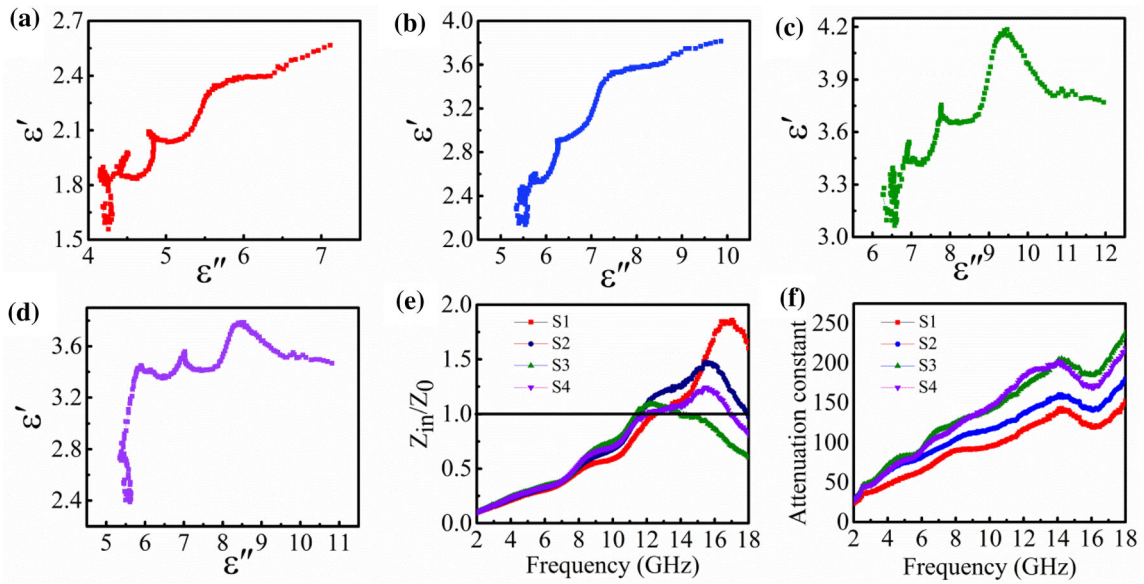

Figure 8 Frequency dependences of **a** real **b** imaginary parts of complex permittivity for S1–S4; **e** the normalized input impedance of the samples at the thickness of 2.0 mm. **f** the attenuation constant of the samples.

outstanding microwave absorption performance. The first is the normalized characteristic impedance matching, which is calculated based on Eq. (2). Normally, a good impedance matching means that electromagnetic waves could successfully enter the absorbers. On the contrary, poor impedance matching can lead to strong electromagnetic reflections [33]. Therefore, in order to make a further study for microwave absorption, the impedance match of all the samples has been calculated and shown in Fig. 8e. It can be observed that the impedance match of S3 is better than the other samples. Good impedance matching for S3 is a precondition to enhance its absorbing performance. Another important factor is the attenuation constant, which is calculated based on the following equation [6, 44]:

$$\alpha = \frac{\sqrt{2}\pi f}{c}\sqrt{(\mu''\varepsilon'' - \mu'\varepsilon') + \sqrt{(\mu''\varepsilon'' - \mu'\varepsilon')^2(\mu''\varepsilon' - \mu'\varepsilon'')^2}} \tag{4}$$

In general, attenuation constant is used to qualify the electromagnetic energy attenuation ability of absorbers. As shown in Fig. 8f, it is obvious that S3 possessed remarkable attenuation capability in the whole frequency range. The result is consistent with the RL and impedance matching analysis, further confirming the superior microwave absorption performance of S3. The microwave absorption properties of other perovskite oxides have been compared with

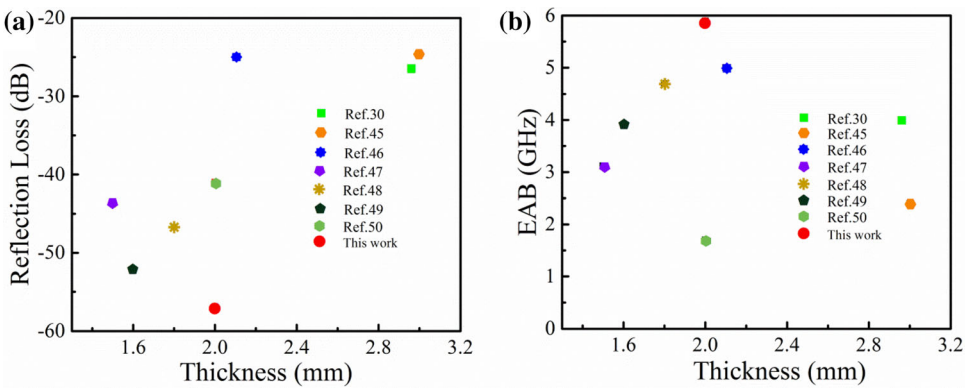

Figure 9 The comparison of microwave absorption between this work and other perovskite oxide absorbers.

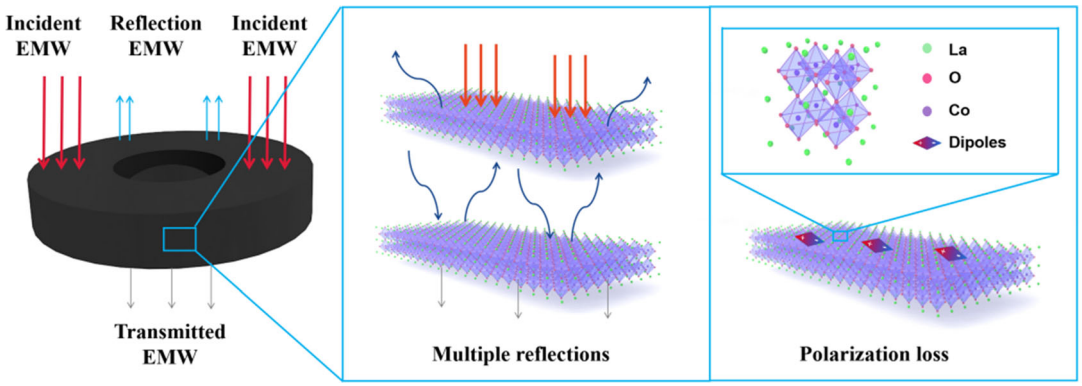

Figure 10 Schematic illustration of the microwave absorption mechanism for $LaCoO_3$ thin sheet *A*-site cation deficiency.

$LaCoO_3$ thin sheets in this work summarized in Fig. 9. In this work, the RL_{min} value of − 56.9 dB at 15.1 GHz can be achieved and a broad effective absorption bandwidth that reaches 5.9 GHz is comparable or even better than those of perovskite oxide absorbers.

According to the analysis above, the corresponding microwave absorption mechanism of $LaCoO_3$ thin sheet *A*-site cation deficiency is illustrated in Fig. 10. First, when the electromagnetic waves are transmitted to the sample, the electromagnetic waves can be reflected back and forth between the $LaCoO_3$ thin sheets, leading to multiple reflections and attenuation. Second, polarization loss plays an important role in the system. Introducing the La defects suitably can induce more dipoles, which can give rise to dipole polarization and relaxation, leading to more dielectric loss. Third, the optimum impedance match characteristic allowed more electromagnetic waves to enter the microwave absorption materials, which is the basis for obtaining an excellent microwave absorption performance.

Conclusions

In summary, the $LaCoO_3$ thin sheets with *A*-site cation deficiency have been successfully obtained by a selectively etching strategy. Importantly, adjusting the amount of $FeCl_3$ to control over introduces the *A*-site cation deficiency, the $LaCoO_3$ thin sheets exhibit excellent microwave absorption performance. The $LaCoO_3$ thin sheets with *A*-site cation deficiency possess an optimum microwave absorption performance with a thin thickness of 2.0 mm. A minimum reflection loss (RL) value of − 56.9 dB at 15.1 GHz can be achieved and a broad effective absorption bandwidth reaches 5.9 GHz, covering the range of 12.1–18.0 GHz. The excellent microwave absorption performance is attributed to the multiple scattering, interface polarization in the thin sheets, and the dipole polarization which is induced by the *A*-site cation deficiency. Therefore, the microwave absorption performance can be effectively improved when the *A*-site cation deficiency is introduced in $LaCoO_3$ thin sheets. It is expected that the $LaCoO_3$ thin sheets

with A-site cation deficiency could be used to design efficient microwave absorption materials.

Acknowledgements

This work was supported by the National Natural Science Foundation of China (51602116, 11904116), Natural Science Foundation of Anhui Province (1708085QB40, 1908085QA36), and Postdoctoral Research Foundation of China (2016M600492).

Declarations

Conflict of interest The authors declare there is no any commercial or associative interest that represents a conflict of interest in connection with the work submitted.

Supplementary Information: The online version contains supplementary material available at https://doi.org/10.1007/s10853-021-06650-2.

References

[1] Xu X, Ran F, Fan Z, Lai H, Cheng Z, Lv T, Shao L, Liu Y (2019) Cactus-inspired bimetallic metal-organic framework-derived 1D–2D hierarchical Co/N-decorated carbon architecture toward enhanced electromagnetic wave absorbing performance. ACS Appl Mater Interface 11(14):13564–13573

[2] Qu B, Zhu C, Li C, Zhang X, Chen Y (2016) Coupling hollow Fe_3O_4–Fe nanoparticles with graphene sheets for high-performance electromagnetic wave absorbing material. ACS Appl Mater Interface 8:3730–3735

[3] Zhang Z, Tan J, Gu W, Zhao H, Zheng J, Zhang B, Ji G (2020) Cellulose-chitosan framework/polyaniline hybrid aerogel toward thermal insulation and microwave absorbing application. Chem Eng J 395:125190

[4] Liu P, Ng VMH, Yao Z, Zhou J, Lei Y, Yang Z, Lv H, Kong LB (2017) Facile synthesis and hierarchical assembly of flowerlike NiO structures with enhanced dielectric and microwave absorption properties. ACS Appl Mater Interface 9:16404–16416

[5] Qiu Y, Lin Y, Yang H, Wang L, Wang M, Wen B (2020) Hollow Ni/C microspheres derived from Ni-metal organic framework for electromagnetic wave absorption. Chem Eng J 383:123207

[6] Wang H, Meng F, Huang F, Jing C, Li Y, Wei W, Zhou Z (2019) Interface modulating CNTs@PANi hybrids by controlled unzipping of the walls of CNTs to achieve tunable high-performance microwave absorption. ACS Appl Mater Interface 11(12):12142–12153

[7] Gu W, Tan J, Chen J, Zhang Z, Zhao Y, Yu J, Ji G (2020) Multifunctional bulk hybrid foam for infrared stealth, thermal insulation, and microwave absorption. ACS Appl Mater Interface 12(25):28727–28737

[8] Gai L, Zhao Y, Song G, An Q, Xiao Z, Zhai S, Li Z (2020) Construction of core-shell PPy@MoS_2 with nanotube-like heterostructures for electromagnetic wave absorption: Assembly and enhanced mechanism. Compos Part A: Appl S 136:105965

[9] Li Y, Liu X, Nie X, Yang W, Wang Y, Yu R, Shui J (2019) Multifunctional organic-inorganic hybrid aerogel for self-cleaning, heat-insulating, and highly efficient microwave absorbing material. Adv Funct Mater 29:1807624

[10] Wang S, Zhang M, Liu Q, Zhang P, Zhang K, Kong X (2018) Synthesis of chain-like α-Fe/Fe_3O_4 core/shell composites exhibiting enhanced microwave absorption performance in high-frequency under an ultrathin matching thickness. J Mater Sci-Mater Electron 29:21040–21050. https://doi.org/10.1007/s10854-018-0250-3

[11] Li Q, Zhu J, Wang S, Huang F, Liu Q, Kong X (2020) Microwave absorption on a bare biomass derived holey silica-hybridized carbon absorbent. Carbon 161:639–646

[12] Xu H, Yin X, Zhu M, Han M, Hou Z, Li X, Zhang L, Cheng L (2017) Carbon hollow microspheres with a designable mesoporous shell for high-performance electromagnetic wave absorption. ACS Appl Mater Interface 9:6332–6341

[13] Ning M, Man Q, Tan G, Lei Z, Li J, Li R-W (2020) Ultrathin MoS2 nanosheets encapsulated in hollow carbon spheres: a case of a dielectric absorber with optimized impedance for efficient microwave absorption. ACS Appl Mater Interface 12:20785–20796

[14] Liu J, Liang H, Zhang Y, Wu G, Wu H (2019) Facile synthesis of ellipsoid-like $MgCo_2O_4$/Co_3O_4 composites for strong wideband microwave absorption application. Compos Part B-Eng 176:107240

[15] Cui X, Liang X, Liu W, Gu W, Ji G, Du Y (2020) Stable microwave absorber derived from 1D customized heterogeneous structures of Fe_3N@ C. Chem Eng J 381:122589

[16] Wang S, Hu K, Huang F, Zhang M, Wu S, Liu Q, Kong X (2019) Activating microwave absorption via noncovalent interactions at the interface based on metal-free graphene nanosheets. Carbon 152:818–826

[17] Shingange K, Swart HC, Mhlongo GH (2020) Design of porous p-type $LaCoO_3$ nanofibers with remarkable response and selectivity to ethanol at low operating temperature. Sens Actuat B-Chem 308:127670

[18] Wang L, Ma T, Dai S, Ren T, Chang Z, Dou L, Fu M, Li X (2020) Experimental study on the high performance of Zr doped $LaCoO_3$ for solar thermochemical CO production. Chem Eng J 389:124426

[19] Qian J, Wang T, Zhang Z, Liu Y, Li J, Gao D (2020) Engineered spin state in Ce doped $LaCoO_3$ with enhanced electrocatalytic activity for rechargeable Zn-Air batteries. Nano Energy 74:104948

[20] Sun M, Zou L, Wang Z, Guo S, Chen Y, Chi B, Pu J, Li J (2019) Porous nanocubes $La_{0.9}Co_{0.8}Ni_{0.2}O_{3-x}$ as efficient catalyst for Li-O2 batteries. Electrochim Acta 327:135017

[21] Liu Y, Kong X, Guo X, Li Q, Ke J, Wang R, Li Q, Geng Z, Zeng J (2019) Enhanced N_2 electroreduction over $LaCoO_3$ by introducing oxygen vacancies. ACS Catal 10:1077–1085

[22] Zhu HY, Zhang PF, Dai S (2015) Recent advances of lanthanum-based perovskite oxides for catalysis. ACS Catal 5:6370–6385

[23] Tan P, Liu ML, Shao ZP, Ni M (2017) Recent advances in perovskite oxides as electrode materials for nonaqueous lithium-oxygen batteries. Adv Energy Mater 7:1–23

[24] Li Q, Liu Q, Kong X (2020) Noncovalent heterointerface on boron-carbon hybrid for improved microwave absorption. J Mater Sci 55:14345–14357. https://doi.org/10.1007/s10853-020-05060-0

[25] Xu X, Wang G, Wan G, Shi S, Hao C, Tang Y, Wang G (2020) Magnetic Ni/graphene connected with conductive carbon nano-onions or nanotubes by atomic layer deposition for lightweight and low-frequency microwave absorption. Chem Eng J 382:122980

[26] Liu P, Gao S, Wang Y, Huang Y, Wang Y, Luo J (2019) Core-shell CoNi@Graphitic carbon decorated on B, N-codoped hollow carbon polyhedrons toward lightweight and high-efficiency microwave attenuation. ACS Appl Mater Interface 11:25624–25635

[27] Chen G, Zhu Y, Chen HM, Hu Z, Hung S-F, Ma N, Dai J, Lin H-J, Chen C-T, Zhou W, Shao Z (2019) An amorphous nickel-iron-based electrocatalyst with unusual local structures for ultrafast oxygen evolution reaction. Adv Mater 31:1900883

[28] Guo Y, Shao T, You H, Li S, Li C, Zhang L (2017) Polyvinylpyrrolidone-assisted solvothermal synthesis of porous $LaCoO_3$ nanospheres as supercapacitor electrode. Int J Electrochem Sci 12:7121–7127

[29] Wang H, Chen X, Huang D, Zhou M, Ding D, Luo H (2020) Cation deficiency tuning of $LaCoO_3$ perovskite as bifunctional oxygen electrocatalyst. ChemCatChem 12:2768–2775

[30] Liu X, Wang L-S, Ma Y, Zheng H, Lin L, Zhang Q, Chen Y, Qiu Y, Peng D-L (2017) Enhanced microwave absorption properties by tuning cation deficiency of perovskite oxides of two-dimensional $LaFeO_3$/C composite in X-band. ACS Appl Mater Interface 9:7601–7610

[31] Yang Q, Wang D, Wang C, Li X, Li K, Peng Y, Li J (2018) Facile surface improved method of $LaCoO_3$ for toluene oxidation. Catal Sci Technol 8:3166–3173

[32] Jia Z, Gao Z, Feng A, Zhang Y, Zhang C, Nie G, Wang K, Wu G (2019) Laminated microwave absorbers of A-site cation deficiency perovskite $La_{0.8}FeO_3$ doped at hybrid RGO carbon. Compos Part B-Eng 176:107246

[33] Xie X, Ni C, Lin Z, Wu D, Sun X, Zhang Y, Wang B, Du W (2020) Phase and morphology evolution of high dielectric CoO/Co_3O_4 particles with Co_3O_4 nanoneedles on surface for excellent microwave absorption application. Chem Eng J 396:125205

[34] Ouyang J, He Z, Zhang Y, Yang H, Zhao Q (2019) Trimetallic FeCoNi@C nanocomposite hollow spheres derived from metal-organic frameworks with superior electromagnetic wave absorption ability. ACS Appl Mater Interface 11:39304–39314

[35] Cheng Y, Cao J, Li Y, Li Z, Zhao H, Ji G, Du Y (2018) The outside-in approach to construct Fe_3O_4 nanocrystals/mesoporous carbon hollow spheres core-shell hybrids toward microwave absorption. Acs Sustain Chem Eng 6:1427–1435

[36] Wang Y, Du Y, Qiang R, Tian C, Xu P, Han X (2016) Interfacially engineered sandwich-like rGO/carbon microspheres/rGO composite as an efficient and durable microwave absorber. Adv Mater Interface 3:1500684

[37] Liu D, Du Y, Xu P, Liu N, Wang Y, Zhao H, Cui L, Han X (2019) Waxberry-like hierarchical Ni@C microspheres with high-performance microwave absorption. J Mater Chem C 7:5037–5046

[38] Deng B, Xiang Z, Xiong J, Liu Z, Yu L, Lu W (2020) Sandwich-like Fe&TiO_2@C nanocomposites derived from MXene/Fe-MOFs hybrids for electromagnetic absorption. Nano-Micro Lett 12:1–16

[39] Guo Y, Li J, Meng F, Wei W, Yang Q, Li Y, Wang H, Peng F, Zhou Z (2019) Hybridization-induced polarization of graphene sheets by intercalation-polymerized polyaniline toward high performance of microwave absorption. ACS Appl Mater Interface 11:17100–17107

[40] Ding D, Wang Y, Li X, Qiang R, Xu P, Chu W, Han X, Du Y (2017) Rational design of core-shell Co@C microspheres for high-performance microwave absorption. Carbon 111:722–732

[41] Xu Z, Du Y, Liu D, Wang Y, Ma W, Wang Y, Xu P, Han X (2019) Pea-like Fe/Fe_3C nanoparticles embedded in nitrogen-doped carbon nanotubes with tunable dielectric/magnetic loss and efficient electromagnetic absorption. Acs Appl Mater Interface 11:4268–4277

[42] Wang X, Zhu T, Chang S, Lu Y, Mi W, Wang W (2020) 3D nest-like architecture of core-shell $CoFe_2O_4$@1T/2H-MoS_2 composites with tunable microwave absorption performance. ACS Appl Mater Interface 12:11252–11264

[43] Quan B, Shi W, Ong SJH, Lu X, Wang PL, Ji G, Guo Y, Zheng L, Xu ZJ (2019) Defect engineering in two common types of dielectric materials for electromagnetic absorption applications. Adv Funct Mater 29:1901236

[44] Zhang X, Wang X, Meng F, Chen J, Du S (2019) Broadband and strong electromagnetic wave absorption of epoxy composites filled with ultralow content of non-covalently modified reduced graphene oxides. Carbon 154:115–124

[45] Yang J, Zhang J, Liang C, Wang M, Zhao P, Liu M, Liu J, Che R (2013) Ultrathin $BaTiO_3$ nanowires with high aspect ratio: a simple one-step hydrothermal synthesis and their strong microwave absorption. ACS Appl Mater Interface 5:7146–7151

[46] Liu S, Luo H, Yan S, Yao L, He J, Li Y, He L, Huang S, Deng L (2017) Effect of Nd-doping on structure and microwave electromagnetic properties of $BiFeO_3$. J Magn Magn Mater 426:267–272

[47] Hu K, Wang S, Zhang M, Huang F, Kong X, Liu Q (2019) Enhanced microwave absorption properties of La doping $BaSnO_3$ ceramic powder. J Mater Sci-Mater Electron 30:15420–15428

[48] Moitra D, Dhole S, Ghosh BK, Chandel M, Jani RK, Patra MK, Vadera SR, Ghosh NN (2017) Synthesis and microwave absorption properties of $BiFeO_3$ nanowire-RGO nanocomposite and first-principles calculations for insight of electromagnetic properties and electronic structures. J Phys Chem C 39:21290–21304

[49] Wang L, Li X, Li Q, Zhao Y, Che R (2018) Enhanced polarization from hollow cube-like $ZnSnO_3$ wrapped by multiwalled carbon nanotubes: as a lightweight and high-performance microwave absorber. ACS Appl Mater Interface 10:22602–22610

[50] Liu Y, Feng Y, Wu X, Han X (2009) Microwave absorption properties of La doped barium titanate in X-band. J Alloy Compd 472:441–445